PHYSICAL REVIEW B **84**, 165412 (2011)

Photoconduction and the electronic structure of silica nanowires embedded with gold nanoparticles

C.-W. Pao,[1,*] C.-T. Wu,[2] H.-M. Tsai,[1,*] Y.-S. Liu,[1] C.-L. Chang,[1] W. F. Pong,[1,†] J.-W. Chiou,[3] C.-W. Chen,[2] M.-S. Hu,[4] M.-W. Chu,[5] L.-C. Chen,[5,‡] C.-H. Chen,[4,5] K.-H. Chen,[4,5] S.-B. Wang,[5,6] S.-J. Chang,[6] M.-H. Tsai,[7] H.-J. Lin,[8] J.-F. Lee,[8] and J.-H. Guo[9]

[1]*Department of Physics, Tamkang University, Tamsui 251, Taiwan*
[2]*Department of Material Science and Engineering, National Taiwan University, Taipei 106, Taiwan*
[3]*Department of Applied Physics, National University of Kaohsiung, Kaohsiung 811, Taiwan*
[4]*Institute of Atomic and Molecular Sciences, Academia Sinica, Taipei 106, Taiwan*
[5]*Center for Condensed Matter Sciences, National Taiwan University, Taipei 106, Taiwan*
[6]*Institute of Microelectronics and Department of Electrical Engineering, National Cheng Kung University, Tainan 701, Taiwan*
[7]*Department of Physics, National Sun Yat-Sen University, Kaohsiung 804, Taiwan*
[8]*National Synchrotron Radiation Research Center, Hsinchu 300, Taiwan*
[9]*Advanced Light Source, Lawrence Berkeley National Laboratory, Berkeley, California 94720, USA*

(Received 25 May 2011; revised manuscript received 30 July 2011; published 7 October 2011)

Silica nanowires (SiO_x-NWs) embedded with Au peapods have been studied by energy-filtered scanning transmission electron microscopy (EFTEM), O *K*- and Au L_3-edge x-ray absorption near-edge structure (XANES), and extended x-ray absorption fine structure (EXAFS), x-ray emission spectroscopy (XES) and scanning photoelectron microscopy. XANES and XES data show that band gaps of Au-peapod-embedded and pure SiO_x-NWs were 6.8 eV. In additional, XANES and EXAFS results indicate illumination-induced electron transfer from Au peapod to SiO_x-NWs and does not show any feature attributable to the formation of Au-Si bonding in the Au peapod embedded in SiO_x-NWs with or without illumination. Photoresponse and EFTEM measurements show that green light has more significant enhancement of photoconductivity than red and blue light due to surface plasmon resonance and suggest that transport of electrons across SiO_x-NWs is via Mott-variable-range hopping mechanism through localized or defect states.

DOI: 10.1103/PhysRevB.84.165412 PACS number(s): 78.70.Dm, 73.20.Mf, 73.22.−f, 78.67.Bf

I. INTRODUCTION

The electromagnetic properties, especially the effect of surface plasmon resonance (SPR),[1,2] of metallic nanoparticles encapsulated in the dielectric matrix are of fundamental and optoelectronics interests. Electron energy-loss spectroscopy (EELS) and scanning transmission electron microscopy have been used to map surface plasmons (SP) in a silver nanoprism,[3] Au peapods in Ga_2O_3 nanowires,[4] Au nanoparticles deposited on lacy carbon films,[5] and Au nanoparticles embedded in silica nanowires (SiO_x-NWs).[6] Hu *et al*. measured photoresponse as resistivity of Au peapods embedded in SiO_x-NWs and found that red- and blue-light irradiation only slightly improved photoconductivity, while green-light irradiation enhanced photoconductivity significantly.[7] Photoconductivity enhancement under green-light irradiation was argued to be due to SPR, because the Au peapod has a pronounced SPR absorption at λ_{ex}=532 nm.[7] Generation of hot electrons and enhancement of the drift (diffusion) current ratio through the SiO_x barrier[8] were regarded as critical in enhancing photoconductivity of Au peapods embedded in silicate. A similar wavelength-dependent photoresponse was also observed in the cysteamine capped colloid Au monolayer.[9] When metallic nanoparticles are irradiated at SPR, an oscillating electric field was argued to cause conduction electrons to oscillate coherently, which affects couplings between electronic states in the host dielectric matrix and conduction electrons.[10] However, exactly how conduction electrons in Au nanoparticles couple with electronic states in host SiO_x-NWs and how this coupling affects photoconductivity has seldom been investigated. In this work, a microscopic view of surface plasmonic field distribution and local electronic structures of Au-peapod-embedded SiO_x-NWs with and without (red, green, and blue light) light illumination have been investigated to understand photoconductivity.

II. EXPERIMENTAL

Au L_3-edge x-ray absorption near-edge structure (XANES) and extended x-ray absorption fine structure (EXAFS) were obtained in the fluorescence mode using the wiggler-17C and scanning photoelectron microscopy (SPEM)-photoemission spectra were obtained using undulator-09A beamlines at the National Synchrotron Radiation Research Center (NSRRC), Hsinchu, Taiwan. The XES and corresponding XANES measurements at the O *K* edge and were carried out in the fluorescence mode at beamline-7.0.1 at the Advanced Light Source, Lawrence Berkeley National Laboratory, and at Dragon-11A beamline at NSRRC. The resolutions were set to ∼0.1 eV (∼1 eV) at photon energies of 530 eV (11.9 keV) during XANES measurements, while the resolution for the XES measurement was set to ∼0.35 eV. The energy scale was calibrated using the spectra of pure Au metal and amorphous SiO_2. All measurements were performed at room temperature. The XANES spectra shown in the figures have been divided by the incident intensity I_0 and are normalized to have the same area in the energy range 550–560 eV for O *K* edge and 11 990–12 800 eV for Au L_3 edge (not fully shown) after following the standard procedure for background subtraction. The energy of SPEM-photoemission spectra was calibrated by the Fermi energy (E_f) of a clean gold metal.

The zero energy is the threshold of the emission spectrum and is referred to as E_f. The Au peapod, pure SiO_x-NWs, and reference Au foil were irradiated by a normally incident solid-state laser, using wavelengths of $\lambda_{ex} = 635$ nm (red), 532 nm (green), and 405 nm (blue) at powers of 25 and 50 mW with spot areas of 4–9 mm^2, respectively. The spectra of those samples under illumination-*on* condition were thus obtained, while the spectra of those samples in the dark (illumination-*off* condition) were also obtained for comparison. The morphology of the samples was characterized by scanning electron microscopy (SEM) before and after the synchrotron radiation measurements were taken, to ensure that irradiation did not damage the samples. Energy-filtered transmission electron microscopy (EFTEM)[11] work was also carried out and was capable of forming an electron probe as small as 0.2 nm. With the small size of a 0.2-nm electron probe (operated at 200 kV) in experiment, the SP excitation of an individual Au nanoparticle can be thoroughly mapped. The EFTEM image is the two-dimensional mapping of the nanostructure using only the electrons which lose a specified amount of energy corresponding to a particular excitation.

Au-peapod-embedded and pure SiO_x-NW samples were grown using microwave-chemical-vapor deposition in a unique sandwiched configuration. Details of preparation and structural characterization of these samples and measurements of their photoresponses are described elsewhere.[7] The ellipsoidal-shaped Au peapods sheathed in the amorphous SiO_x-matrix with a mean diameter of 35±15 nm and interparticle distances of 100–200 nm were determined using SEM and high-resolution transmission electron microscopy. A histogram for the particle size distribution of Au nanoparticle embedded in the SiO_x matrix based on the SEM can be seen in Fig. 1.

A single-wire study of the above phenomena regarding the photoconductivity enhancement was performed using a dual-gun focus ion beam to write the Pt contacts as shown in Fig. 2(a). Figure 2(b) also displays photoresponse of the single-wire device to $\lambda_{ex} = 532$ nm laser illumination with different laser powers, which shows a linear response to the illumination power as depicted in the inset.

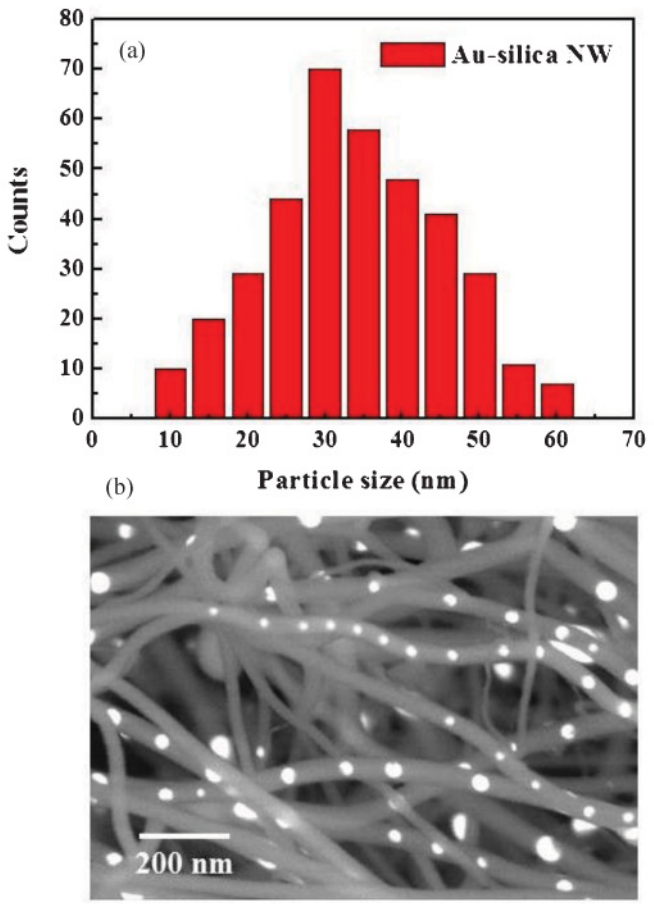

FIG. 1. (Color online) (a) A histogram for the particle size distribution of Au nanoparticles embedded in the SiO_x-NWs based on the SEM (b).

III. RESULTS AND DISCUSSION

The present study examined field distribution in the sample by using EFTEM to further verify enhancement of

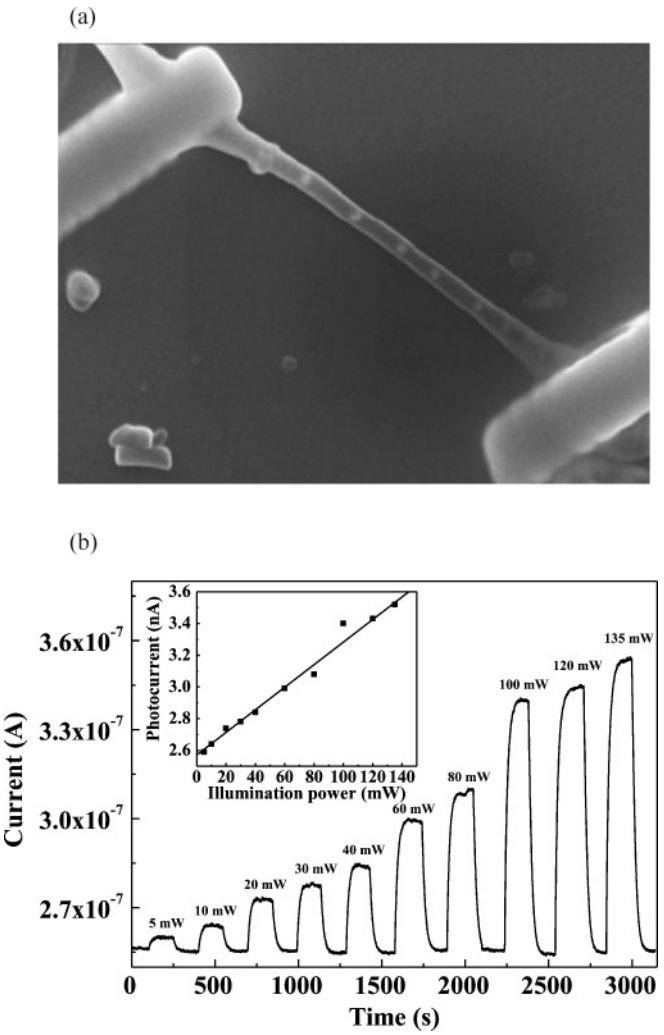

FIG. 2. (a) SEM image of a single SiO_x-NW embedded with Au nanoparticles. (b) Photocurrent versus measurement time, which is divided into periods of illumination-on and illumination-off conditions of different illumination powers at 532 nm with the inset showing the power dependence of the photocurrent.

photoconductivity in Au peapods. A particular Au nanoparticle embedded in the SiO_x matrix was selected. Figure 3(a) shows the pristine EFTEM image of SP field intensity distribution in the energy range 2–4 eV, which covers SPR of the Au nanoparticle. Figure 3(a) shows that the SP field extends all the way to the SiO_x-NW surface. A higher intensity field is observed outside rather than inside the Au-embedded NW and is shown as a brighter stripe on the NW surface in Fig. 3(a). To correctly describe the SP field distribution, the field intensity is normalized by the unscattered electron beam intensity during the EELS measurement as explained in the previous study.[6] This is because the EELS signal is strongly attenuated through SiO_x-NW and no attenuation occurs in the vacuum outside of SiO_x-NW. The corrected-EFTEM image [Fig. 3(b)] and the line scans of intensity profile from the EFTEM images before and after corrections [Fig. 3(c)] clearly reveal that at SPR, the SP intensity, which is the flux of electrons coming out of a given position in the Au-peapod-embedded SiO_x-NW with energies within 2–4 eV, is still substantial inside the silicate matrix, although it decays from the Au-silicate interface into the vacuum. Figure 3(c) shows the continuous distribution of the normalized SP field intensity along the path marked in Fig. 3(b). The decay length of the SP intensity across SiO_x-NW from the Au particle surface L shown in Fig. 3(c) is ~20 nm, which is much smaller than the interdistance between Au nanoparticles of more than 100 nm. Thus, direct electromagnetic coupling between adjacent Au nanoparticles at SPR can be ruled out.

Next, an attempt is made to elucidate the photoconductivity enhancement mechanism by performing synchrotron radiation measurements to explore the correlation between photoconductivity and the electronic structures of the Au peapods embedded in the SiO_x-NWs. Figure 4 and the inset show normalized Au L_3-edge XANES spectra, which correspond to Au $2p_{3/2}$ to $5d/6s$ transitions,[12] of Au peapods and foil, respectively, with and without irradiation under various wavelengths at powers of 25 and 50 mW. Figure 4 and the inset show that the general absorption features of the Au peapod resemble those of the Au foil. Difference near-edge spectra for the Au peapod and foil are displayed at the bottom of Fig. 4 and inset, respectively, which shows that the difference spectra between illumination-on and illumination-off conditions are

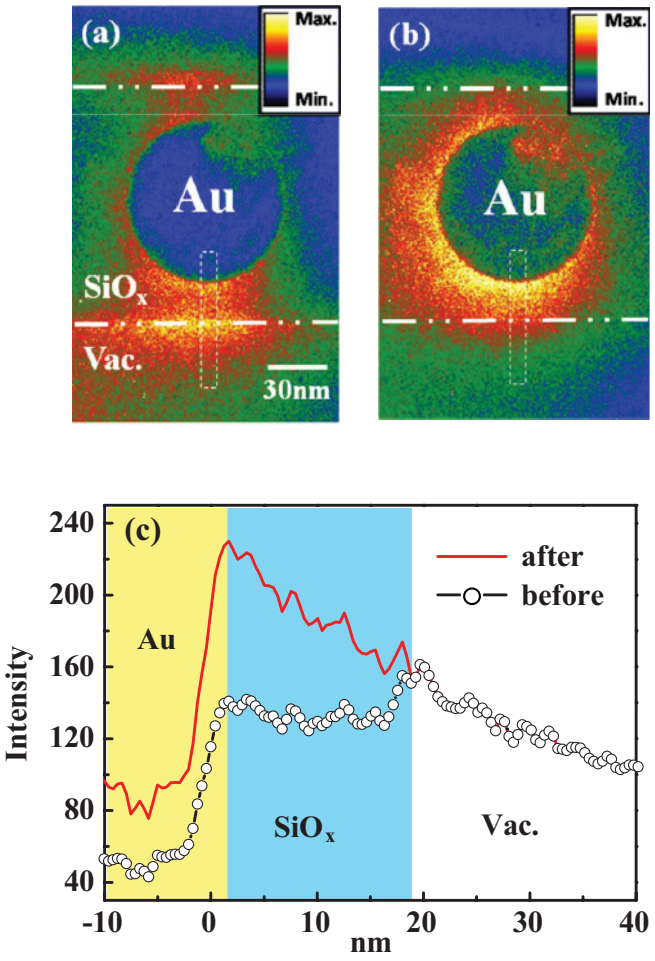

FIG. 3. (Color online) EFTEM image and SP intensity profiles of Au-peapod-embedded SiO_x-NWs within an energy window of 2–4 eV (a) before and (b) after EELS-signal attenuation correction; (c) the line scan of intensity profiles along paths marked by the dashed elongated rectangles shown in (a) and (b).

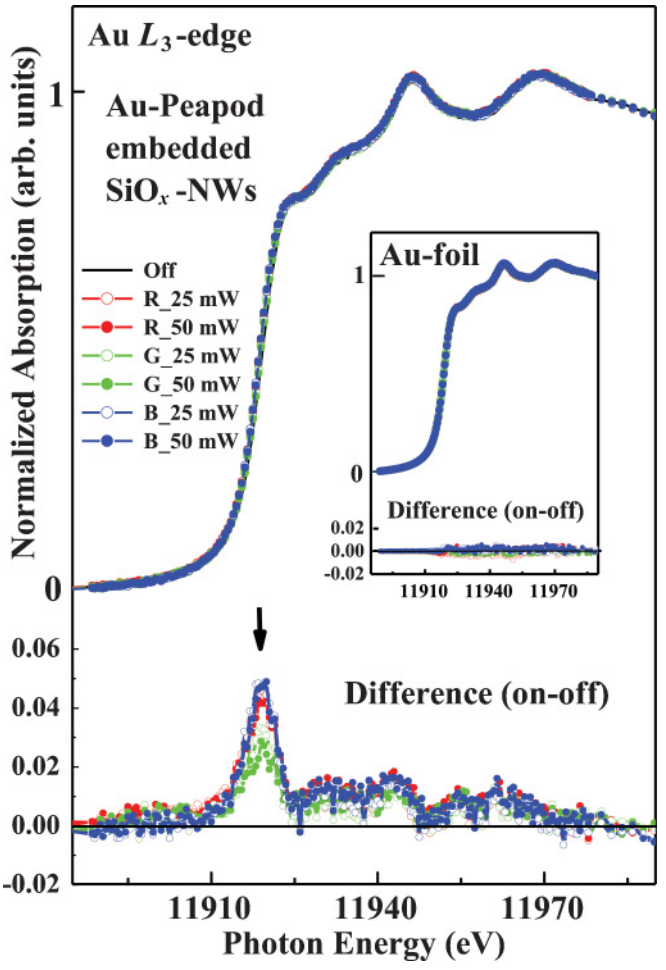

FIG. 4. (Color online) Au L_3-edge XANES spectra of Au-peapod-embedded SiO_x-NWs with and without light illumination using various wavelengths at powers of 25 and 50 mW. The inset shows XANES spectra of Au foil as references. The lower panel displays difference near-edge spectra between illumination-on and illumination-off conditions.

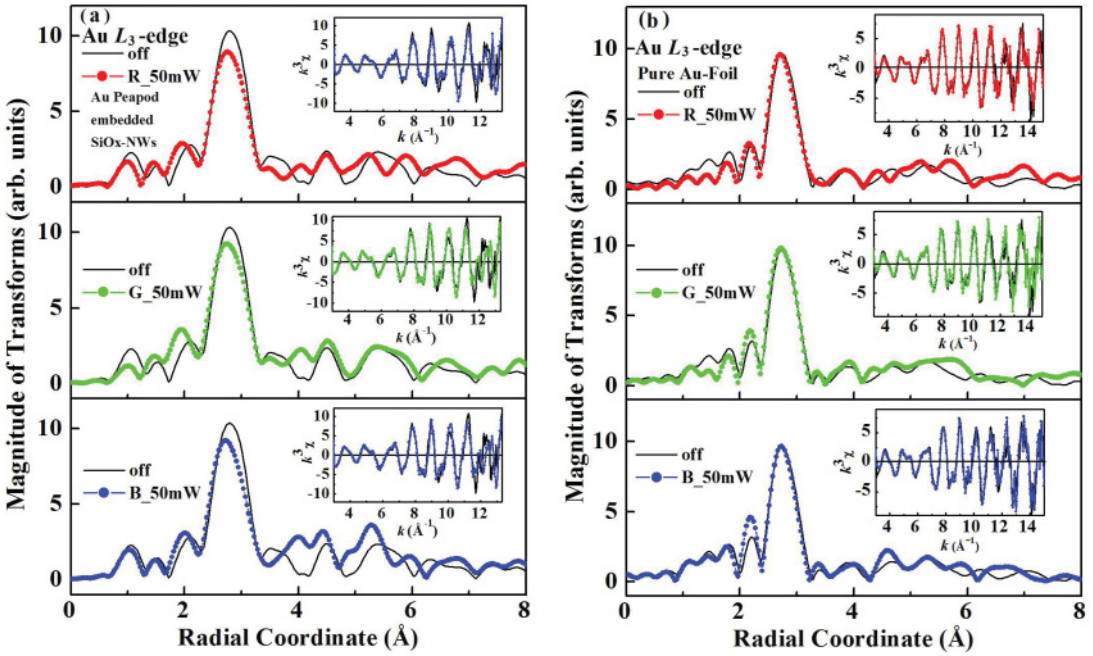

FIG. 5. (Color online) (a), (b) Magnitude of FT of EXAFS $k^3\chi$ at Au L_3 edge of the Au peapod and foil, respectively, from k=3.5 to 13.9 Å^{-1}. Colored circles represent excitation under various wavelengths labeled as R_50 mW, G_50 mW, and B_50 mW with a power of 50 mW. The illumination-off cases are represented by black solid lines. The insets present Au L_3-edge EXAFS oscillation $k^3\chi$ data.

significant for the Au peapod embedded in SiO_x-NWs, but insignificant for the foil. At the threshold region denoted by an arrow, Fig. 4 shows illumination-induced enhancement of unoccupied Au 5*d*/6*s* partial density of states (DOSs), which was argued by Jonnard *et al.*[13] to be related to an increase in the amount of Au-Si binding due to a thermal effect that causes an electron transfer from Au to Si atoms in Au silicides. To quantitatively obtain the information of local atomic structures of Au peapod embedded in SiO_x-NWs requires the analysis using the UWXAFS code, which involves a combination of multiple-scattering EXAFS computer program FEFF[14] and nonlinear least-squares-fitting computer program FEFFIT.[15] Figure 5 and Table I display the Fourier transform (FT) spectra and the results of analysis of the Au L_3-edge EXAFS, respectively. The results of local atomic structures do not show any feature attributable to the Au-Si bond, excluding the formation of Au-Si bonding in the Au peapod embedded in SiO_x-NWs with or without illumination. Enhancement of unoccupied Au 5*d*/6*s* DOSs indicates electron transfer from Au nanoparticles to silicate matrix.

Figure 6 presents normalized O *K*-edge XANES spectra of Au-peapod-embedded SiO_x-NWs obtained with and without illumination with various wavelengths at powers of 25 and 50 mW, which are similar to those of amorphous SiO_2.[16] Broad feature $\mathbf{A_1}$ and that of pure SiO_x-NWs shown in the upper inset can be attributed to antibonding O 2*p*-derived states. The bottom of Fig. 6 displays difference intensity of near-edge features of Au-peapod-embedded SiO_x-NWs between illumination-on and illumination-off conditions, indicating illumination reduced DOSs of unoccupied O 2*p*-derived states. In contrast, the intensity of feature $\mathbf{A_1}$ did not change significantly for pure SiO_x-NWs as shown in the bottom of the upper inset. The negative difference intensity of feature $\mathbf{A_1}$ in the spectra of Au-peapod-embedded SiO_x-NWs overall is insensitive to the power and wavelength of illumination. The reduced O *K*-edge spectral intensities suggest that Au-peapod-induced enhancement of the occupation of O 2*p* states, which is consistent with the Au L_3-edge result that suggests electron transfer from the Au peapod to SiO_x-NWs, occurs when the Au peapod was irradiated.

Figure 7(a) displays XES and corresponding XANES spectra of O 2*p* states of Au-peapod-embedded and pure SiO_x-NWs obtained with and without irradiation with various wavelengths at a power of 50 mW. The maximum intensity of the feature in the XANES spectra was arbitrarily normalized to unity. XES and XANES spectra in Fig. 7(a) resemble those of thin-film SiO_2 presented elsewhere.[17] Features $\mathbf{A_2}$ and $\mathbf{B_2}$ in the O K_α emission spectra are dominated by O 2*p* and O 2*p*-Si 3*sp* hybridized states,[18,19] respectively. Theoretical calculations[20] and experimental photoelectron spectra[21] indicate that states near the conduction-band minimum (CBM) and valence-band

TABLE I. Structural parameters of the Au peapod and foil. N is the corresponding coordination number, R is the nearest-neighbor Au-Au bond length, and σ^2 is the Debye-Waller factor.

Samples	N	R (Å)	$\sigma^2(\times 10^{-3}$ Å$^{-2})$
Au-peapod illumination-off	12	2.90 ± 0.02	8.5 ± 0.5
R_50 mW	12	2.88 ± 0.02	9.2 ± 0.5
G_50 mW	12	2.88 ± 0.02	9.1 ± 0.5
B_50 mW	12	2.88 ± 0.02	9.2 ± 0.5
Au-foil illumination-off	12	2.85 ± 0.01	8.4 ± 0.5
R_50 mW	12	2.85 ± 0.01	8.6 ± 0.5
G_50 mW	12	2.85 ± 0.01	8.5 ± 0.5
B_50 mW	12	2.85 ± 0.01	8.5 ± 0.5

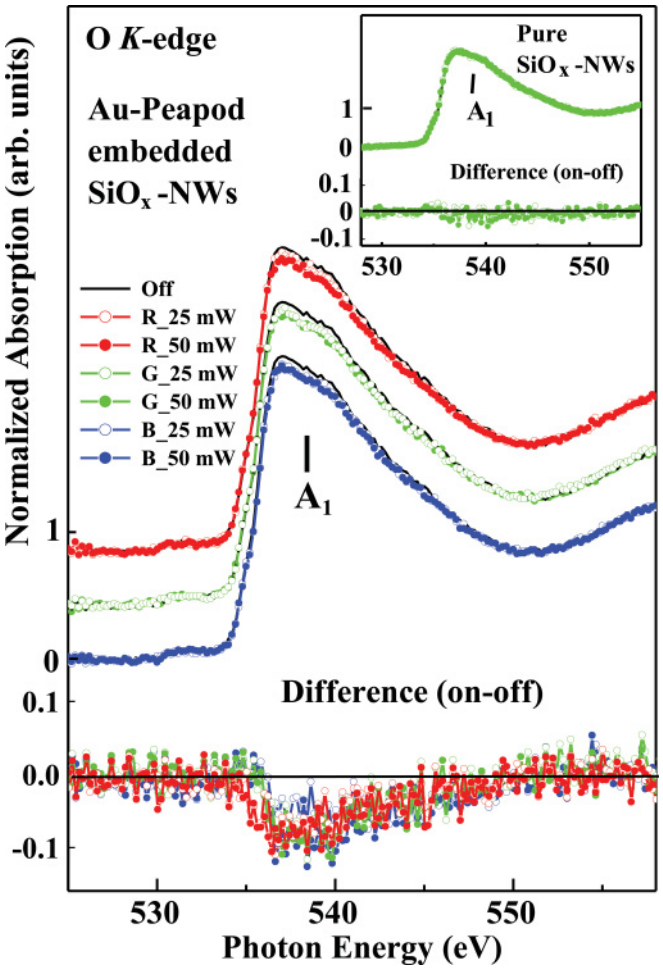

FIG. 6. (Color online) O *K*-edge XANES spectra of Au-peapod-embedded SiO_x-NWs with and without light illumination using various wavelengths at powers of 25 and 50 mW. The inset shows XANES spectra of pure SiO_x-NWs as references. The lower panel displays difference near-edge spectra between illumination-on and illumination-off conditions.

maximum (VBM) of SiO_2 are dominated by antibonding- and bonding-O 2*p* states, respectively. By extrapolating the main edges in the O *K*-edge XANES and O K_α XES spectra to the baselines,[12] which correspond to CBM and VBM of the Au peapod and pure SiO_x-NWs under illumination-on and illumination-off conditions. Figure 7(a) shows a well-defined band gap E_g marked by the two dashed lines. E_g is 6.8 ± 0.1 eV for both Au-peapod-embedded and pure SiO_x-NWs. In comparison, calculated E_g for crystalline and amorphous SiO_2 varied between ~5.6 and 8.8 eV.[17,19,22]

Previous photoresponse measurements revealed that irradiation by green light significantly increases photoconductivity of the Au peapod, while illumination with red or blue light improves photoconductivity only slightly.[7] The physical origin of the dependence of photoconductivity of the Au peapod embedded in SiO_x-NWs on the wavelength or photon energy of irradiation is to be discussed in the following. First, it is assumed that SiO_x is *n* type and an Au-SiO_x Schottky barrier is formed at the interface represented in Fig. 7(b), in which E_f, $q\Phi_B$, $q\Phi_w$ and $q\chi_e$ are the Fermi level, barrier height of the junction, work function of the Au nanoparticle, and electron affinity of silica, respectively. If there is no interface state, $q\Phi_B = q\Phi_w - q\chi_e$.[23] VBM was determined to be –10.6 eV relative to the vacuum level for amorphous SiO_2.[24] With a 6.8-eV band gap, CBM is –3.8 eV relative to the vacuum level and $q\chi_e = 3.8$ eV. In contrast, Ibach and Rowe concluded that $q\chi_e = 1.7$ eV based on a band gap of 8.9 eV.[24] An Au metal has a $q\Phi_w$ of 5.1 eV.[25] Since Au nanoparticles are expected to have more loosely packed high index surfaces, $q\Phi_w$ should be smaller, i.e., $q\Phi_w < 5.1$ eV, which suggests $q\Phi_B < 1.3$ eV for the Au-nanoparticle/SiO_x interface. Then, $q\Phi_B$ is smaller than the photon energies of incident light [1.9 (red), 2.3 (green), and 3.1 eV (blue)] considered in this study. Thus, for all three wavelengths of the incident light, photon-absorbing near-E_f electrons in Au nanoparticles can overcome the Schottky barrier and move into conduction-band states in silica in disagreement with the observation of insignificant enhancement of photoconductivity by red- and blue-light illumination. Thus, the assumption of the formation of the Schottky barrier at the interface was not the case.[26,27]

The common E_f or chemical potential of a metal-*n*-type-semiconductor interface can be pinned at the metal-induced gap state (MIGS) as presented in Fig. 7(c), which is normally located in the middle of the band gap of semiconductors due to charge neutrality.[23,28] MIGS is associated with Bloch-like wave functions $\psi(z)$'s in the metal, which tail exponentially into the forbidden gap of the semiconductor.[23] If this was the case, the potential barrier resulting from the charge transfer to line up E_f is approximately $E_g/2$ or 3.4 eV, which is larger than the photon energies of all the three wavelengths of incident light considered in this study, so that illumination-excited electrons in Au nanoparticles cannot move directly into the conduction band of silica except via tunneling,[29] which explains why illumination even with a blue light does not significantly increase photoconductivity. Thus, the formation of MIGS does not account for present observations.

Shi *et al.* described three types of electronic transport, namely conduction in itinerant, band-tail, and partially filled localized states at E_f.[30] When the excitation energy is sufficiently high, electrons can move from the Au peapod into the itinerant states of SiO_x-NWs and their movement across SiO_x-NWs will resemble those of conduction electrons in metals. However, this was not the case as discussed previously. On the other hand, electrons in band-tail or partially filled localized states near E_f usually have larger effective masses and their movement can be enhanced by phonon-assisted thermally activated hopping mechanism. However, SPEM valence-band photoemission data (Fig. 8) of both Au-peapod-embedded and pure SiO_x-NWs for illumination-on (red, green, and blue light) and illumination-off conditions at powers of 25 and 50 mW do not differ considerably in the vicinity of E_f, which suggests that the valence-band DOSs near or at E_f are insensitive to light illumination even for green illumination at SPR. Thus, photoconductivity enhancement was not due to near-E_f band-tail or partially filled localized states. Thus, the three types of electron transport stated above cannot explain the present experimental observations.

Achatz *et al.* proposed that the conduction mechanism in nitrogen-containing ultrananocrystalline diamond film can

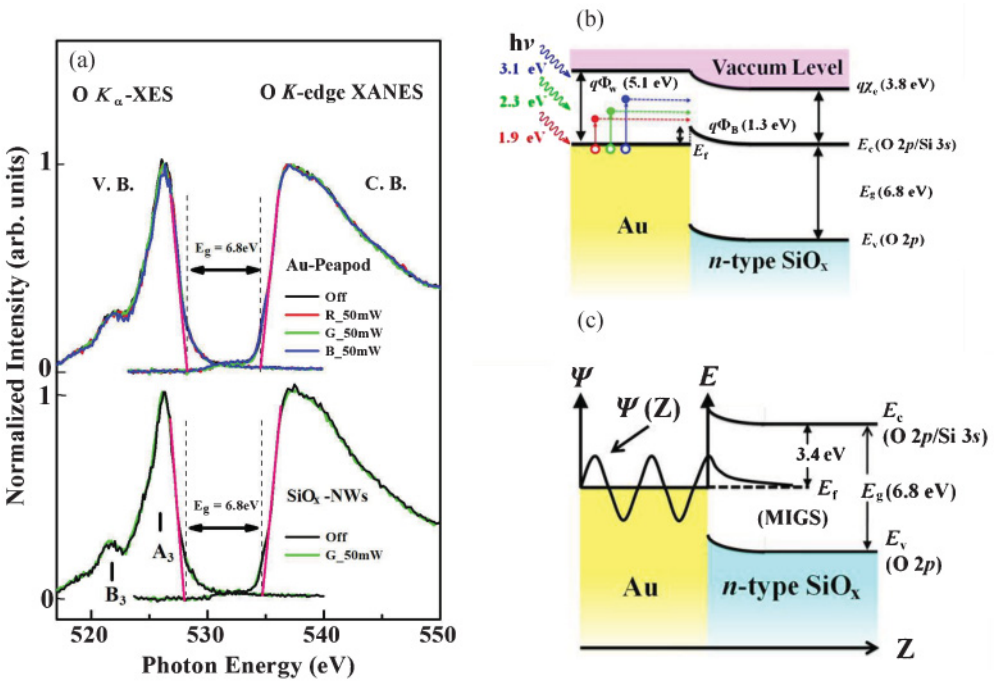

FIG. 7. (Color online) (a) Band-gap determination from XES and XANES spectra of O 2*p* states of Au-peapod-embedded and pure SiO_x-NWs under illumination using various wavelengths at a power of 50 mW and without illumination. (b), (c) Schematic drawings of the band profile of the Au-(*n*-type)SiO_x system with a Schottky barrier and the presence of MIGS, respectively.

be explained by variable-range hopping (VRH) transport via near-E_f localized or defect states.[31] Mott stated that the transition probability from an occupied localized state at one site to an unoccupied localized state at another site separated by a hopping distance R_{ij} depends on the overlapping of the wave functions of these two localized states and the

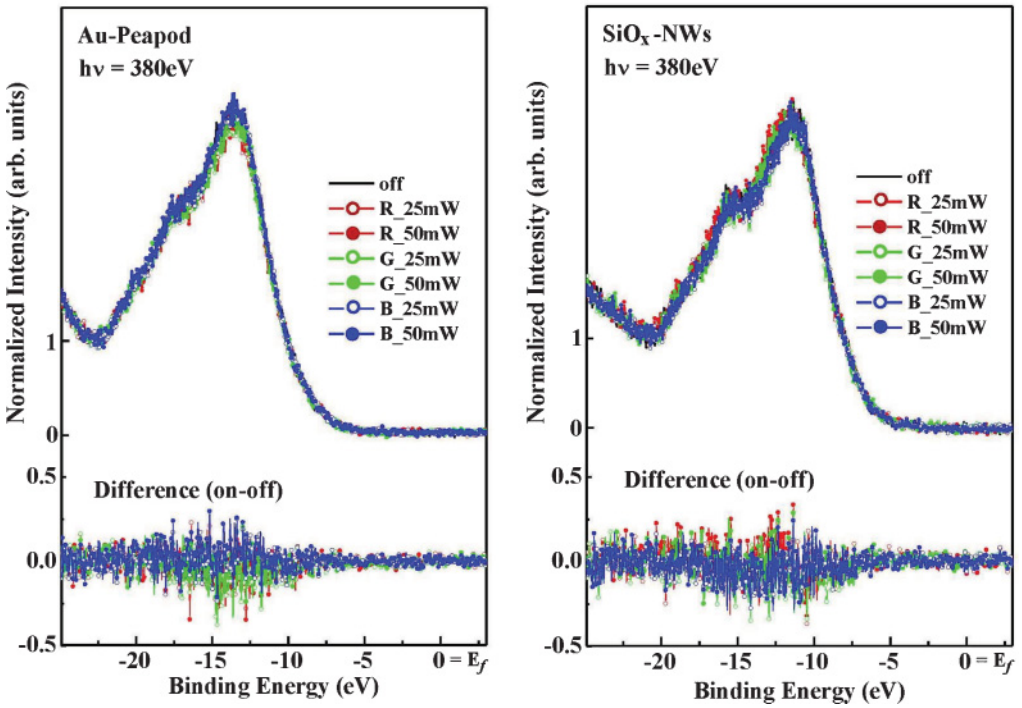

FIG. 8. (Color online) SPEM valence-band photoemission spectra of (a) SiO_x-NWs embedded with Au peapods and (b) pure SiO_x-NWs samples. Valence-band photoemission spectra were obtained with and without illumination at an excited energy of 380 eV. The lower panels display difference valence-band spectra of SiO_x-NWs embedded with Au peapods and pure SiO_x-NWs between illumination-on at powers of 25 and 50 mW and illumination-off conditions. The Fermi level is indicated as E_f.

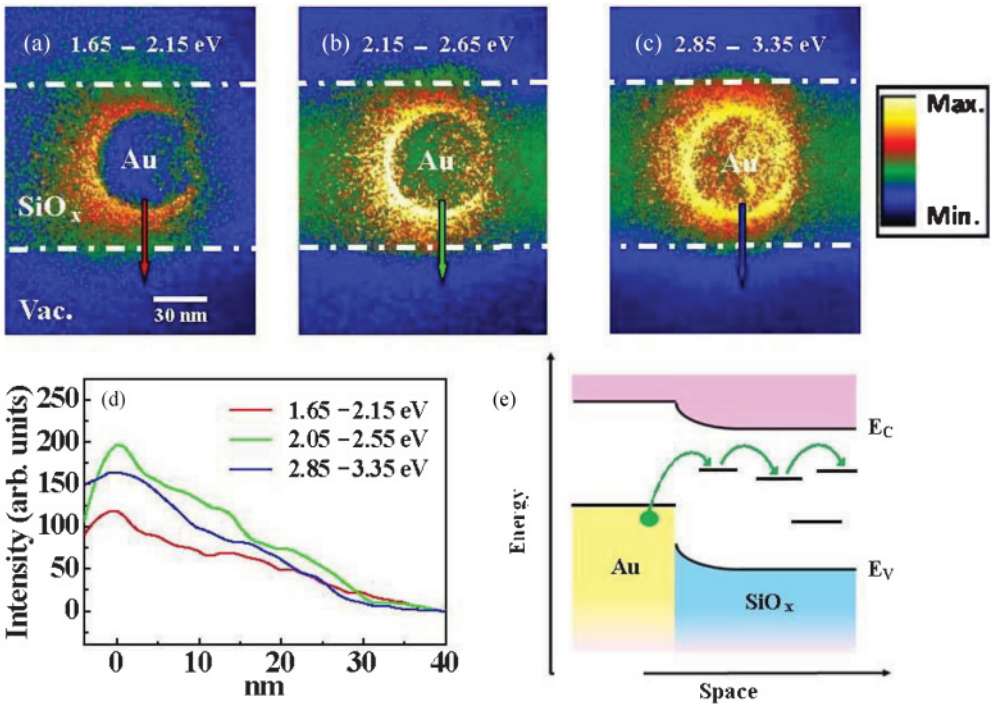

FIG. 9. (Color online) EFTEM images and SP intensity profiles with three selected energy windows of (a) 1.65–2.15, (b) 2.05–2.55, and (c) 2.85–3.35 eV after EELS-signal attenuation correction. (d) Line scans of intensity profiles along the lines marked by arrows in the three EFTEM images (a)–(c). (e) Electron transition diagram illustrating the possible of localized (defect) sites (represented by horizontal lines in the band gap) for hopping conduction at SPR.

potential barrier E between them. The transition probability Γ can be expressed as $\Gamma \propto \exp(-2\alpha R_{ij})\ \exp(-\frac{\Delta E}{k_B T})$.[32] The first exponential term describes an overlapping integral between wave functions of the two localized or defect states with a decay parameter of α, whose inverse $\xi = 1/\alpha$ is known as the decay length,[33,34] which has the same order as the decay length L of SP from the Au nanoparticle surface into SiO_x-NW. Figure 3(c) shows that L is $\sim$20 nm, so $\xi \approx$ 20 nm. In general, the hopping conductivities depend not only on the material parameters but also on the sample temperature as well. Different hopping-conductivity mechanisms, such as thermal delocalization of carriers, nearest-neighbor hopping, Mott-variable-range hopping (Mott-VRH), and Efors-Shklovskii-VRH (ES-VRH), occur in different temperature ranges.[33] For the Mott-VRH (three-dimensional) model, the conductivity can be expressed by the following relation:

$$\sigma(T) = \sigma_0 \exp\left[-\left(\frac{T_o}{T}\right)\right]^{1/4},$$

where T_o is the characteristic Mott temperature. The logarithm plot of the conductivity as a function of $T^{-1/4}$ for a single Au-silica NW suggests the Mott-VRH mechanism is the dominant mechanism for hopping conductivity in Au-silica NW in the temperature range between 77 and 300 K.[35] Within the Mott-VRH model, the hopping distance R_{ij} was estimated to have an order of 10 nm for amorphous silicon.[36,37] If silicate has a higher defect concentration, then R_{ij} is smaller and $\exp(-2R_{ij}/\xi) > \sim 0.4$. If ΔE is large with respect to the thermal excitation energy, Γ will be too small for the hopping mechanism to occur. However, if the photon energy is sufficient large, photoexcited electrons in the Au peapod may move into higher-energy localized or defect states in SiO_x-NW on sites near the Au-peapod/SiO_x-NW interface with a smaller ΔE, and Γ can be significant. Then, it is plausible that photoexcited electrons can move across the Au-peapod/SiO_x-NW interface into unoccupied localized or defect states in SiO_x-NW and migrate across SiO_x-NW via the hopping mechanism.

EFTEM was further performed using energies filtered at 1.65–2.15, 2.05–2.55, and 2.85–3.35 eV corresponding to red, green, and blue excitation energies and are shown in Figs. 9(a)–9(c), respectively. In each measurement, the same energy window step of 0.5 eV was used. The qualities of these images are not as good as those shown in Fig. 3 using a 2-eV energy step owing to the limitation of the EELS system. Figure 9(d) shows line scans of intensity profiles along the lines marked by arrows shown in Figs. 9(a)–9(c). In Fig. 9(d), the background intensity, which is the average intensity in the range 39–40 nm, has been subtracted from the intensities of the three excitations. The EFTEM intensities overall decrease with the order of 2.05–2.55 eV (green), 2.85–3.35 eV (blue), and 1.65–2.15 (red), though blue illumination has a larger photon energy than that of green illumination. The largest intensity for green illumination clearly is due to SPR, which gives rise to a larger flux of excited electrons than those of red and blue illumination and outweighs the effect of larger excitation energy for blue illumination that causes electrons to move into higher-energy localized or defect states in SiO_x-NW with a larger Γ. Figure 9(e) indicates a possible transition diagram of localized sites for hopping conduction at SPR. The *non*-SPR red and blue illumination have a smaller transition or hopping probability and consequently smaller photoconductivity.

IV. CONCLUSION

In summary, Au L_3- and O K-edge XANES measurements suggest the existence of illumination-induced electron transfer from Au peapods into SiO_2-NWs. XANES and XES data show that band gaps of Au-peapod-embedded and pure SiO_x-NWs were the same, 6.8 eV. Photoresponse and EFTEM measurements show that green light has more significantly enhances photoconductivity than red and blue light due to SPR and suggest that transport of electrons across SiO_x-NWs is via Mott-VRH mechanism through localized or defect states.

ACKNOWLEDGMENTS

W.F.P. would like to thank the National Science Council of Taiwan for financially supporting this research under Contract No. NSC 99-2119-M032-004-MY3. M.S.H. would like to acknowledge the postdoctoral fellowship sponsored by Academia Sinica, Taiwan.

*Present address: National Synchrotron Radiation Research Center, Hsinchu 300, Taiwan.
†wfpong@mail.tku.edu.tw
‡chenlc@ntu.edu.tw

[1] U. Kreibig and M. Vollmer, *Optical Properties of Metal Cluster* (Springer, Berlin, 1995).
[2] F. J. Garcia de Abajo, Rev. Mod. Phys. **82**, 209 (2010).
[3] J. Nelayah, K. Mathieu, S. Odile, F. J. Garcia de Abajo, T. Marcwl, H. Luc, T. Dario, P. S. Isabel, M. L. M. Luis, and C. Christian, Nature Phys. **3**, 348 (2007).
[4] C. H. Hsieh, L. J. Chou, G. R. Lin, Y. Bando, and D. Golberg, Nano Lett. **8**, 3081 (2008).
[5] M. W. Chu, C. H. Chen, F. J. Garcia de Abajo, J. P. Deng, and C. Y. Mou, Phys. Rev. B **77**, 245402 (2008).
[6] C. T. Wu, M. W. Chu, S. B. Wang, M. S. Hu, K. H. Chen, L. Y. Chen, C. W. Chen, and C. H. Chen, Appl. Phys. Lett. **96**, 263106 (2010).
[7] M. S. Hu, H. L. Chen, C. H. Shen, L. S. Hong, B. R. Huang, K. H. Chen, and L. C. Chen, Nat. Mater. **5**, 102 (2006).
[8] K. Berthold, R. A. Hopfel, and E. Gornik, Appl. Phys. Lett. **46**, 626 (1985).
[9] Y. Jin and N. Friedman, J. Am. Chem. Soc. **127**, 11902 (2005).
[10] E. Hutter and J. H. Fendler, Adv. Mater. **16**, 1685 (2004).
[11] M. W. Chu, V. Myroshnychenko, C. H. Chen, J. P. Deng, C. Y. Mou, and F. J. Garcia de Abajo, Nano Lett. **9**, 399 (2009).
[12] J. W. Chiou, S. C. Ray, H. M. Tsai, C. W. Pao, F. Z. Chien, W. F. Pong, M. H. Tsai, J. J. Wu, C. H. Tseng, C. H. Chen, J. F. Lee, and J. H. Guo, Appl. Phys. Lett. **90**, 192112 (2007).
[13] P. Jonnard, H. Bercegol, L. Lamaignere, J. P. Morreeuw, J. L. Rullier, E. Cottancin, and M. Pellarin, J. Appl. Phys. **97**, 064306 (2005).
[14] J. J. Rehr, J. Mustre de Leon, S. I. Zabinsky, and R. C. Albers, J. Am. Chem. Soc. **113**, 5135 (1991).
[15] A. I. Frenkel, E. A. Stern, M. Qian, and M. Newville, Phys. Rev. B **48**, 12449 (1993).
[16] H. M. Tsai, S. C. Ray, C. W. Pao, J. W. Chiou, C. L. Huang, C. H. Du, W. F. Pong, M. H. Tsai, A. Fukano, and H. Oyanagi, J. Appl. Phys. **103**, 013704 (2008).
[17] C. McGuinness, D. Fu, J. E. Downes, K. E. Smith, G. Hughes, and J. Roche, J. Appl. Phys. **94**, 3919 (2003).
[18] G. Wiech, H. O. Feldhütter, and A. Šimůnek, Phys. Rev. B **47**, 6981 (1993).
[19] M. Z. Huang and W. Y. Ching, Phys. Rev. B **54**, 5299 (1996).
[20] T. H. DiStefano and D. E. Eastman, Phys. Rev. Lett. **27**, 1560 (1971).
[21] S. T. Pantelides and W. A. Harrison, Phys. Rev. B **13**, 2667 (1976).
[22] T. Tamura, S. Ishibashi, S. Tanaka, M. Kohyama, and M. H. Lee, Phys. Rev. B **77**, 085207 (2008).
[23] S. R. Elliott, *The Physics and Chemistry of Solids* (John Wiley & Sons Ltd., Chichester, UK, 1998).
[24] H. Ibach and J. E. Rowe, Phys. Rev. B **10**, 710 (1974).
[25] C. T. Tseng, Y. H. Cheng, M. C. M. Lee, C. C. Han, C. H. Cheng, and Y. T. Tao, Appl. Phys. Lett. **91**, 233510 (2007).
[26] Y. Tian and T. Tatsuma, J. Am. Chem. Soc. **127**, 7632 (2005).
[27] H. Han, N. D. Theodore, and T. L. Alford, J. Appl. Phys. **103**, 013708 (2008).
[28] J. Tersoff, Phys. Rev. B **32**, 6968 (1985).
[29] M. S. Son, J. E. Im, K. K. Wang, S. L. Oh, Y. R. Kim, and K. H. Yoo, Appl. Phys. Lett. **96**, 023115 (2010).
[30] X. Shi, H. Fu, J. R. Shi, L. K. Cheah, B. K. Tay, and P. Hui, J. Phys.: Condens. Matter **10**, 9293 (1998).
[31] P. Achatz, O. A. Williams, P. Bruno, D. M. Gruen, J. A. Garrido, and M. Stutzmann, Phys. Rev. B **74**, 155429 (2006).
[32] N. Mott, *Conduction in Non-Crystalline Materials*, 2nd ed (Oxford Science Publications, New York, 1993).
[33] V. F. Gantmakher, *Electrons and Disorder in Solids* (Clarendon Press, Oxford, 2005).
[34] R. A. Street, *Hydrogenated Amorphous Silicon* (Cambridge University Press, Cambridge, 1991).
[35] S. B. Wang *et al.* (unpublished).
[36] A. Lewis, Phys. Rev. Lett. **29**, 1555 (1972).
[37] D. K. Paul and S. S. Mitra, Phys. Rev. Lett. **31**, 1000 (1973).